Collisions between Small Precipitation Drops. Part I: Laboratory Measurements of Bounce, Coalescence, and Temporary Coalescence

HARRY T. OCHS III, KENNETH V. BEARD,* ROBERT R. CZYS, NEIL F. LAIRD, DANIEL E. SCHAUFELBERGER,† AND DONNA J. HOLDRIDGE#

Cloud and Precipitation Research, Illinois State Water Survey, Champaign, Illinois

(Manuscript received 15 August 1994, in final form 30 December 1994)

ABSTRACT

Self-collection efficiencies were measured for isolated drop pairs falling at terminal velocity using orthogonal cameras to obtain the horizontal offset of the drops before collision and the collision outcome. Data were obtained on four different drop-size pairs over a range of impact Weber number (1–10) and size ratio (0.45–0.73). Collision offsets and outcomes were recorded during 45 experiment runs as a function of drop charge. The collision results from all 4200 events were tabulated by offset and charge, and the coalescence efficiency was determined for each run as a function of charge.

Collision results revealed a coalescence region for small offset and a bounce region at intermediate-to-large offset and low-to-intermediate charge. The critical offset that separated the regions of coalescence and bounce was independent of charge. At higher values of charge, increasing charge was found to induce permanent and/or temporary coalescence from smaller and larger offsets until bounce was completely eliminated. In the offset range for temporary coalescence, the filament connecting the separating drops often collapsed into one and, occasionally, two satellite drops. Mean satellite sizes of 58–81-μm radius were generally consistent with previous measurements using colliding drop streams. The production of satellite drops by colliding precipitation drops should provide precipitation embryos that would accelerate the accretion of cloud water in warm-base convective clouds.

Coalescence efficiencies of 15%–55% at minimal charge were significantly lower than previously reported for smaller drops; therefore, the results indicate a further reduction in the growth rate of precipitation drops. The efficiencies did not vary in a simple way with either Weber number or size ratio. For a constant size ratio ($p \approx 0.7$) the coalescence efficiency decreased with increasing Weber number, whereas for a constant Weber number (We $\approx$ 4.2) the coalescence efficiency decreased with increasing size ratio. An excellent fit to the laboratory coalescence efficiencies, using the theoretical scaling for inelastic collisions, is presented in a companion paper. The resulting formulas for precipitation drops will allow application of these findings to self collection, a process that controls the spreading of raindrops to larger sizes and the growth of radar reflectivity.

1. Introduction

Collisions between small precipitation drops are believed to play an important role in the development of rain by controlling the spread of precipitation drops to larger sizes. This process has been identified as "self-collection" in the stochastic collection calculations of Berry and Reinhardt (1974a,b). The coalescence efficiency for model calculations must be obtained in the laboratory, because theory is woefully inadequate for describing the off-center collisions between deformable drops in a gas.

Earlier lab studies of drop collisions have relied on collisions between continuous streams of drops from water jets (Gunn 1965; Sartor and Abbott 1972; Park 1970; Brazier-Smith et al. 1972). Results that would apply to precipitation drops are limited to a few size pairs having the appropriate velocity. Even these few results may be affected by the wakes of neighboring drops in the stream (e.g., see Pruppacher and Klett 1978).

In our laboratory work, we have measured self-collection efficiencies for isolated drop pairs falling at terminal velocity. Our first study showed that direct collisions produced permanent coalescence and indirect collisions resulted in bounce (Ochs et al. 1986; Czys 1987), lowering the collection efficiency by as much as 60%. In our subsequent study of larger sizes we found separation after coalescence (i.e., temporary coalescence) occurring for indirect collisions at low drop

* Also affiliated with the Department of Atmospheric Sciences, University of Illinois at Urbana Champaign, Champaign, Illinois.

† Current affiliation: ENSR Consulting & Engineering, Westmont, Illinois.

Current affiliation: Argonne National Laboratory, Argonne, Illinois.

Corresponding author address: Harry Ochs, Illinois State Water Survey, 2204 Griffith Drive, Champaign, IL 61820.
E-mail:K-beard@uiuc.edu

charge, temporary coalescence with satellite production at moderate charge, and permanent coalescence for most collisions at high charges (Czys and Ochs 1988). In three later experiments on other size pairs we found similar behavior, but the critical offset between coalescence and bounce (i.e., coalescence efficiency) varied with drop size (Schaufelberger 1990; Ochs et al. 1991; Holdridge 1992; Laird 1992). Herein, we evaluate our experimental observations of collisions between small precipitation drops for the size pairs that we have investigated. Our findings will be used in a companion paper to develop a physically based scaling of the coalescence efficiency to assess self collection over a wider range of drop sizes (Beard and Ochs 1995).

2. Background

The interaction of precipitation drops is conveniently divided into a collision and a coalescence stage. In the collision stage the relative motion of the drops is controlled by aerodynamics. An evaluation of the collision stage is usually obtained by numerical calculation of the drop trajectories as a function of the initial horizontal offset between drop centers (x) to find the largest offset (x_0) for a collision. The collision efficiency for freely falling drops is the fraction of drops that collide having initial offsets within the collision geometry:

$$E = x_0^2/(R + r)^2, \tag{1}$$

where R and r are the radii of the large and small drops.

The collision stage is simplified for precipitation drops because the collision cross section is geometric ($x_0 = R + r$) when the large drop is greater than 50-μm radius and the size ratio ($p = r/R$) is in the range $p = 0.1$–0.9 (e.g., see Pruppacher and Klett 1978). Numerical calculations show that drops of these sizes and size ratios do not accelerate appreciably before they collide (Almeida 1977; Shafrir and Gal-Chen 1971); therefore, the large and small precipitation drops collide at their differential fall speed $\Delta V = V - v$.

The coalescence stage is set by the impact parameters as depicted in Fig. 1. The outcome of a collision for a particular size pair, such as coalescence or bounce, varies with the horizontal offset (x). The offset can also be expressed as the contact angle, $\theta = \sin^{-1}[x/(R + r)]$, shown in Fig. 1. In laboratory studies the collision-coalescence outcomes are measured as a function of offset so that an overall evaluation of the coalescence stage can be specified by a coalescence efficiency giving the fraction coalesced for all possible collisions. The coalescence efficiency for the simple case of a central region of coalescence and an outer region of bounce is defined by the largest coalescence offset (x_c):

$$\epsilon = [x_c/(R + r)]^2 = \sin^2\theta_c. \tag{2}$$

This coalescence efficiency gives the coalescence cross section, and, therefore, the fraction of coalescences for a particular size pair undergoing collisions having random horizontal spacing in two dimensions. The coalescence efficiency is the critical parameter for calculating the growth rate of precipitation drops in the self-collection regime. It is the only unknown in the kernel for the stochastic collection equation

$$K(R, r) = E\epsilon\pi(R + r)^2\Delta V \tag{3}$$

because r, R, and ΔV are specified and the collision cross section is geometric ($E = 1$).

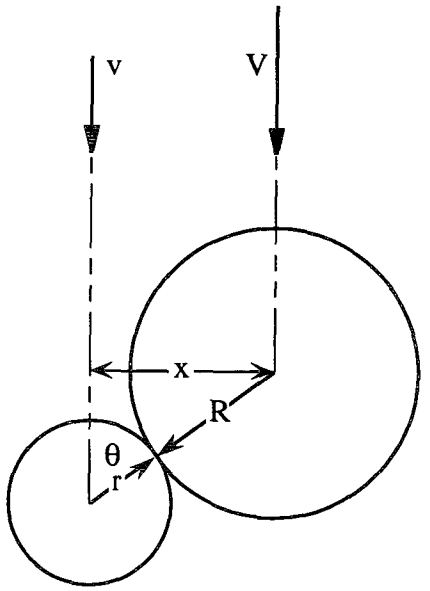

FIG. 1. Schematic of impact geometry showing offset (x) and impact angle (θ) for drops of radii R, r colliding at terminal speeds V, v.

Colliding precipitation drops have a characteristic impact energy that can be calculated from the drop masses and impact velocity ($\Delta V = V - v$). The impact energy is a key parameter for scaling the collision outcomes, such as coalescence efficiency, as a function of drop size (e.g., see Beard and Ochs 1984). In this paper we use a dimensionless form of the impact energy (or pressure) called the Weber number:

$$\text{We} = \rho r\Delta V^2/\sigma, \tag{4}$$

where ρ is the water density and σ is the surface tension. This parameter will be used along with drop sizes and size ratios to help categorize our laboratory observations of bounce, coalescence, and temporary coalescence.

Studies using colliding drop streams by Howarth and Crosby (as given in Park 1970) and also by Sartor and Abbott (1972) have shown that coalescence is enhanced for drops of similar sizes having charges found in warm rain and thunderstorms. Even though these results are not directly applicable to falling drops, they indicate that the effect of electric charge should be in-

cluded in studies of drop interactions in the self-collection regime.

To characterize the charge on the large drop (Q) and small drop (q), we used the magnitude of the relative charge:

$$\Delta Q = |Q - q| \tag{5}$$

found by Howarth and Crosby to scale the suppression of bounce. Because the electric field between nearly touching drops of similar size scales with ΔQ (Davis 1964), the outwardly directed electric stresses on adjacent surfaces of approaching drops also scale with ΔQ. Therefore, the bridging between drops should be promoted by higher values of ΔQ.

3. Experiment

Measurements of the collision characteristics for small precipitation drops were based initially on the design of Adam et al. (1971), whereby drop pairs were produced from a single generator and the interactions recorded with a single camera. The experiment was improved using digital circuitry to control the drop production and to trigger the camera and strobe (Ochs and Beard 1978) with results reported by Ochs et al. (1986). Because the sizes and charges using a single drop generator could not be independently controlled and the collision geometry could not be completely determined, the experiment was upgraded to dual drop generators and orthogonal cameras (Ochs and Czys 1987). The key feature of the improved experiment was an IBM-compatible PC computer with an interface for governing digital timing circuits to control the drop generators, cameras, and strobes. The PC was also used to display and record the experiment parameters, and for computing the distance needed for drops to reach terminal velocity.

The results of the four studies reported here are from the theses of Czys (1987), Schaufelberger (1990), Holdridge (1992), and Laird (1992) that have utilized the computer-controlled drop generation and data acquisition system reported in Ochs and Czys (1987). In each of these studies the collision trajectories and outcomes (e.g., coalescence, bounce, temporary coalescence) were recorded for a particular size pair interacting at terminal velocity. Data were accumulated on 4200 interactions to help determine the effect of charge and relative humidity on parameters, such as the coalescence efficiency, that influence the growth of precipitation drops.

The diagram in Fig. 2 shows a side view of the experiment components and a top view of the cameras, lighting, and drop generators. The apparatus consisted of two computer-controlled drop generators with separate charging electrodes, resting on a column of clear acrylic chambers. The upper chamber contained the high-voltage deflection electrodes and the lower one served as a fall column with sensor ports for an elec-

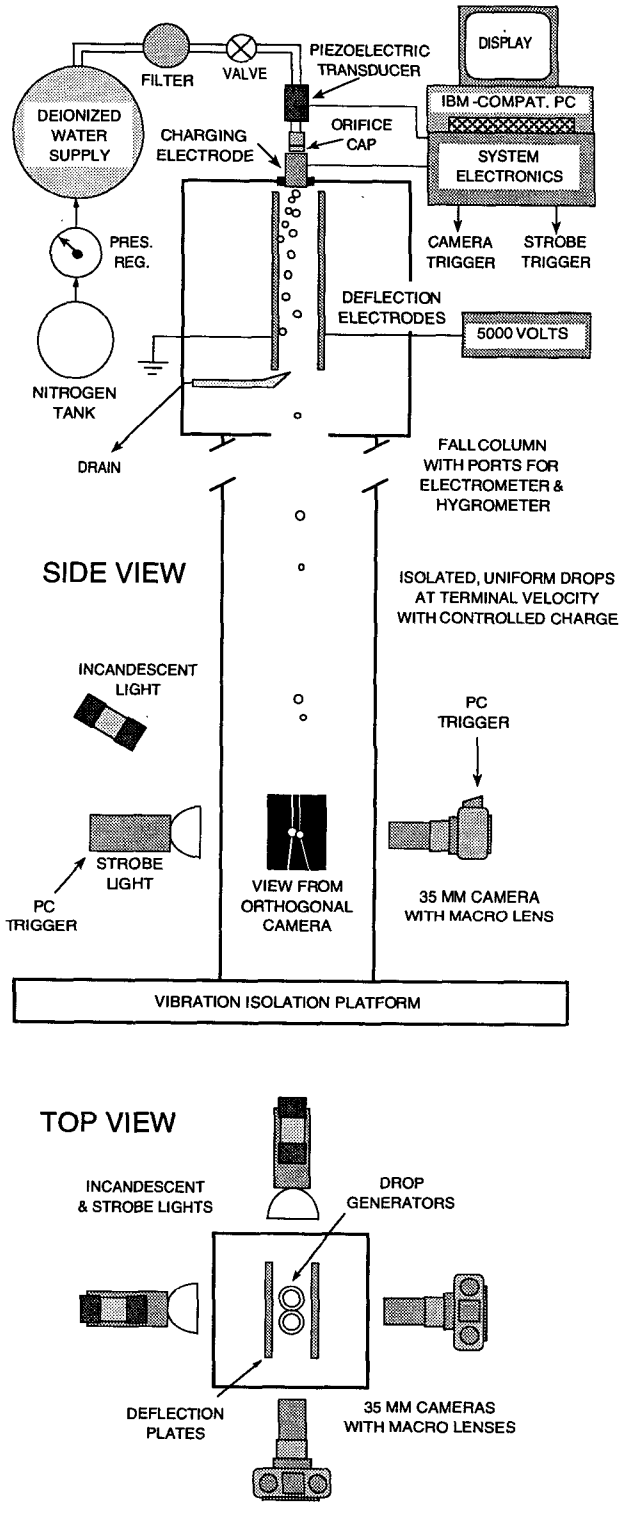

FIG. 2. Side view of experiment chamber and components, and top view of cameras and lighting.

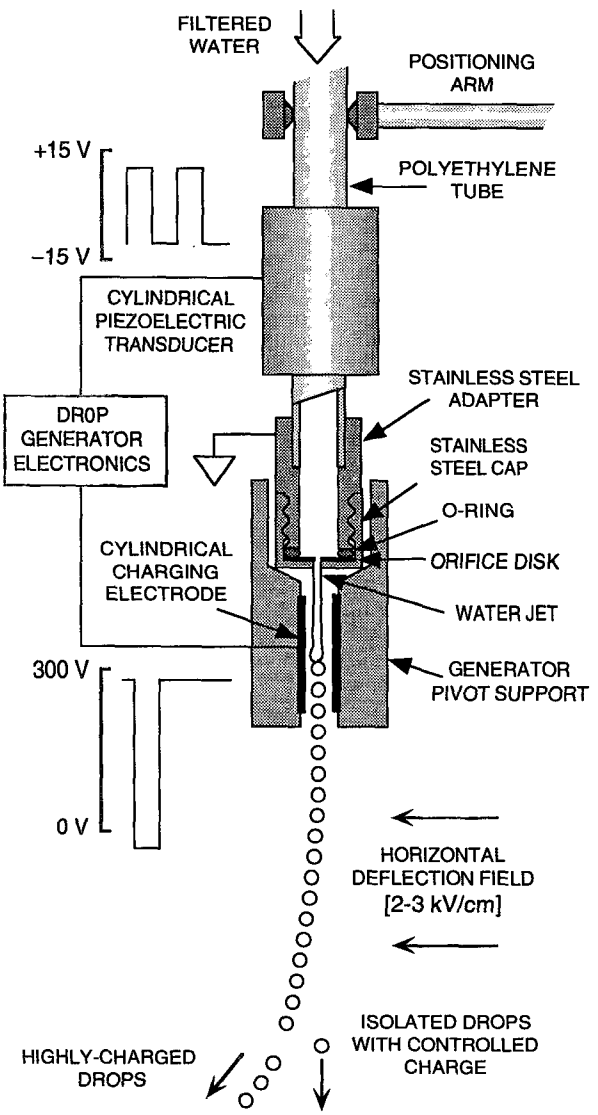

FIG. 3. Schematic of drop generator showing transducer, charging electrode, and voltage pulses. Drop production is illustrated by cross section of orifice holder and pivot support. Positioning arm is attached to a 2D micromanipulator.

trometer and hygrometer. Drop collisions were recorded near the bottom of the lower chamber. The experiment rested on an isolation platform to minimize interference from vibrations. Each drop generator was supplied from its own pressure-regulated reservoir located on a separate isolation platform (not shown). An aluminum frame resting on the floor (not shown) supported the lighting and camera equipment as well other instruments for measuring temperature, humidity, and drop charge.

a. Drop generation

Deionized water was supplied from separate 55-gallon polyethylene-lined drums through polyethylene tubing and 0.2-μm filters to provide contaminant-free water for drop production. The drums were supported sideways to minimize the change in water level and hydrostatic pressure during an experiment. Water flowed into the generator assembly (Fig. 3), exiting through an orifice to form a liquid jet. Radial vibrations on the piezoelectric transducer, induced by a square-wave voltage, produced flow modulations in the jet. The resulting capillary waves caused the jet to separate into a stream of uniformly sized drops.

The drop mass from each generator was determined by weighing an amount of water collected for a prescribed time and dividing by the transducer frequency. Because the major error in mass was in the timing, and was no worse than 0.5 in 60 s (0.8%), the error in the radius was no more than 0.3%.

Once the desired drop sizes were obtained, the drop streams were charged. The generators were positioned so that breakup of the jets occurred near the midlevel of the charging electrode (Fig. 3) to provide good electrical coupling to the drops. The charged drops then passed between the high-voltage plates and were deflected by a strong horizontal field of about 3 kV cm^{-1}. These drops were collected and drained from the chamber. A computer-controlled switching circuit was used to apply a pulse of reduced voltage to each charging electrode so that drops from each stream fell as "pulsed-out" pairs between the plates without significant deflection. To achieve the charge switching, it was necessary to decrease the charge relaxation time of the jet by doping the water with sodium nitrate ($<$100 ppm). This low concentration had a negligible effect on water density, viscosity, and surface tension.

The speed of the drops below the deflection chamber was measured using a strobe and traveling microscope to obtain the vertical displacement between flashes. The pressure regulators were adjusted to alter the jet speed so that the drops would be close to the terminal velocity at the cameras [typically within 1% as determined from acceleration theory, Beard (1977)]. The flow rate was measured before and after each experiment run to insure that the drop sizes and speeds had not changed significantly.

The generator assemblies were attached to separate micromanipulators to control the fall trajectories and cause frequent collisions between drops in view of the cameras. To achieve collisions between charged drops, the generators were tilted slightly so that the pulsed-out drops had minimal horizontal velocity when they emerged from the deflection plates. The generators were mounted as close together as possible (about 1 cm apart), to obtain nearly vertical trajectories. With this arrangement, the angle between drop generator and collision point was less than 0.5°.

b. Data collection

Interactions were recorded by 35-mm cameras viewing the drop collisions from orthogonal directions (Fig.

2). Digital-recording camera backs provided the time on each frame to the nearest second. This insured that frames containing collisions from each camera could be matched during analysis. An incandescent lamp was positioned 30° above each camera axis. Against a darkened background the image of the lamp in each drop provided a trace of their trajectories on the film, and allowed for measurement of the separation of their centers before collision (Fig. 1).

A stroboscopic light was placed on each camera axis to obtain a backlit image of the collision. The strobe intensity was reduced so that the film could still register streaks. To photograph the drop interactions, the height of the collisions and the triggering of the strobes and cameras were adjusted through the computer interface (Fig. 2). The combined streak-strobe record from each camera provided the data needed to determine the collision geometry and outcome.

Charge measurements were obtained using a laboratory-built FET-input electrometer. Drops in the fall column were intercepted by the electrometer sensor and the output pulses captured by a digital oscilloscope. A computer was used to read and integrate the pulses to obtain drop charges. Adjustments were made to the charging electrodes to obtain the desired drop charges before collisions were recorded on each roll of film. At the end of each roll, the charges were measured again, so that the film could be discarded if the charges had drifted appreciably.

The smallest charge that could be readily maintained on the drops was in the range 0.001–0.01 pC (1 pC $= 10^{-12}$C). Because of drop-to-drop variations of up to a factor of 2, the low-charge measurements were determined to just one significant figure. At higher charges ($\geq$0.01 pC) the uncertainty was small enough to represent the charges by two significant figures.

For studies at high relative humidity the chambers were sprayed with deionized water and sealed. The low-humidity studies were conducted in winter months by continuously purging the chambers with room air when the relative humidity was below about 30%. During each of the humidity experiments, the measurement chamber was monitored by a dewpoint hygrometer.

c. *Data analysis*

After the photographic data were developed, the individual frames were inspected using a hand magnifier to identify the type of collision. The observed streak signatures are shown schematically in Fig. 4. A pair of straight fall paths indicated a miss (M), a single streak below the interaction was the signature of complete coalescence (C), and fall paths that diverged below the interaction indicated a bounce (B). Streaks became modulated by drop oscillations directly below the interactions, providing evidence that the drops had collided. This signature was helpful in distinguishing subtle bounces from misses. Streaks that crossed below the collision indicated rotation, which was a signature of temporary coalescence (T). One and two additional streaks below the collision signified temporary coalescence events that produced satellite drops (T_1, T_2). The strobe image disclosed that the satellites formed from the collapsing neck as drops separated. The strobe also helped to distinguish a bounce from a temporary coalescence with weak rotation having a streak signature similar to B in Fig. 4.

The horizontal separation just above the each collision was determined from the film by using a microscope with a micrometer eyepiece. The measurements were aided by the vertical filar (spider thread) that was used to smooth the graininess at the edges of streaks. To compensate for differences in streak width, two separations were measured: one between the right edges of the two streaks and the other between the left edges. The average gave the separation between drop centers, as projected on film, without bias from the width of the streaks. These measured separations were converted to distance in μm using a factor obtained from photographs of a scale with 0.5-mm divisions. The true offset between centers before each collision was calculated from the orthogonal views by $x = (x_1 + x_2)^{1/2}$, where x_1 and x_2 are the separations measured from each camera.

The microscope procedures were carefully established for each new experimenter. Repeated measurements of the same frame were occasionally done to verify that separations could be reproduced to better than 2 μm. Streaks that were too fuzzy to meet this criterion were not measured. As a result, the rms error in offset measurements was 2 μm. The micrometer was also used to measure the diameter of satellite drops that were in focus and relatively undistorted by oscillations.

The number of coalescence, bounce, and temporary coalescence (with number of satellites) was tabulated by offset within intervals corresponding to $^1/_{25}$ the col-

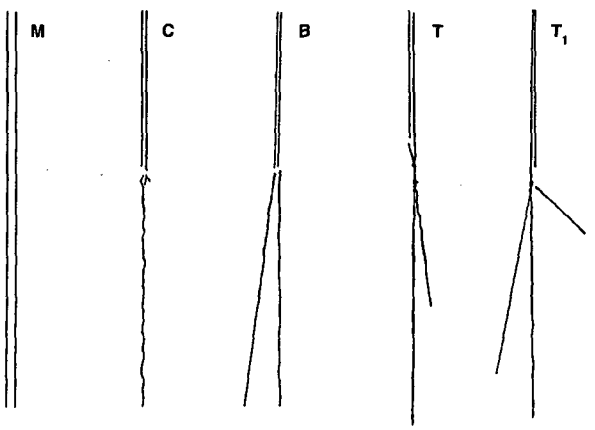

FIG. 4. Schematic of fall streaks showing miss (M), coalescence (C), bounce (B), and temporary coalescence without (T) and with one (T_1) satellite drop (after Czys and Ochs 1988).

lision cross section: $\Delta A = \pi(R + r)^2/25$. The offset boundaries, x_m ($m = 1-25$), were obtained from

$$x_m^2 = (R + r)^2 m/25. \quad (6)$$

Because each category contains $1/25$th of the collision cross section, $x_m^2 - x_{m-1}^2 = (R + r)^2/25$, the probability of observing a collision was the same in any category, assuming that the drops were spaced randomly in the two horizontal dimensions of offset.

The relative charge magnitude $\Delta Q = |Q - q|$ is the simplest parameter that scales the effect of charge-induced coalescence, so an average ΔQ was obtained from the measured values of $|Q - q|$ for each experimental run. The single value of ΔQ for each drop-size, drop-charge pair was the mean ΔQ from all the experimental runs for that pair. The 95% confidence interval in the mean values of ΔQ was typically $\pm 0.1 \Delta Q$, except in some of the lowest charge cases. The "certainty" is given explicitly in the results by specifying ΔQ to one or two significant figures.

4. Results

a. Collision outcomes

Table 1 shows the parameters in the four thesis studies arranged by increasing Weber number and decreasing size ratio. The range in Weber number was We = 1.1–9.6, in the size ratio was $p = 0.47-0.73$, and in large drop size was $R = 275-425$ μm. In our previous study (Ochs et al. 1986), the Weber numbers and drops sizes were smaller (We = 0.033–1.6, $R = 128-308$ μm). In the present study an average of 70–110 collision events were recorded during an experiment with the drop charges and humidities held constant. For each drop pair the charges were varied over a wide range. The relative humidity was maintained near saturation ($\geq$95%), except in the low relative humidity experiments conducted by Schaufelberger (30%), Holdridge (38%), and Laird (21%, 23%, 30%, 32%). A total of 4200 collisions were analyzed from over 1000 rolls of film obtained during the 45 experiments. All the collision outcomes from the four studies are tabulated in the appendix.

The collision outcomes for some example experiments from the lower Weber number study of Schaufelberger are given in Table 2. This table is arranged by increasing relative charge, showing number of coalescences (C) and bounces (B) in 25 equal cross sections by increasing offset. In all experiments, the most direct collisions resulted in coalescence (i.e., for offsets categories ≤ 9, impact angles $\leq 36°$). For the lowest charge, the collisions at larger offset resulted in bounce. With increasing charge, the offset region of bounce was eliminated by charge-induced coalescence from the direction of both larger and smaller offsets.

Representative experiments from the higher Weber number study of Laird are given in Table 3, and show temporary coalescence (T) with one or two satellites (T_1, T_2), in addition to coalescence (C) and bounce (B). As in the study of Schaufelberger, the most direct collisions resulted in coalescence, and the region of bounce was reduced by coalescence from both larger and smaller offsets as the charge increased. In the case of Laird, however, most of the charge-induced coalescences were temporary, except at the highest charges.

To simplify comparison between the studies, the collision outcomes are shown schematically in Figs. 5–8 using different patterns to represent coalescence, bounce, and temporary coalescence (with or without satellites). The outcomes were arranged using a vertical logarithmic scale of increasing relative charge (ΔQ) for outcomes in 25 equal cross sections on the horizontal scale. The corresponding experiment numbers are shown on the left and impact angles at the top. Only the majority outcome is shown at each offset. Thus, many of the outcome regions actually overlap, especially at transition between outcomes. The results were extended vertically to meet the experiments at lower and higher charges at the indicated experiment boundaries. A more detailed description of the outcome patterns is given in the appendix along with a discussion of the experimental uncertainties.

Figures 5–8 show that coalescence is a general feature of the most direct impacts at all charge levels. At larger offsets there is a region of bounce in all four studies at lower charges that was transformed into coalescence and/or temporary coalescence at higher charge. In the lowest Weber number study (Fig. 5) the effect of charge was to induce permanent coalescences. As the charge increased, the offset region of bounce was eliminated by charge-induced coalescence from the direction of larger offset. This phenomenon was noted by Howarth and Crosby (see Park 1970) and further discussed by Ochs et al. (1991).

TABLE 1. Parameters for self-collection experiments by increasing Weber number and decreasing size ratio, giving drop sizes, relative charge magnitude ($\Delta Q = |Q - q|$), relative humidity (RH), and number of experiments and recorded events.

	R (μm)	r (μm)	We	p	ΔQ (pC)	RH (%)	Expts.	Events
Schaufelberger	275	200	1.14	0.73	0.003–0.26	30, $\geq$95	8	726
Laird	425	300	4.22	0.71	0.001–4.7	21–32, $\geq$95	16	1749
Czys	340	190	4.25	0.56	0.009–2.1	$\geq$95	13	910
Holdridge	425	200	9.60	0.47	0.003–4.6	38, $\geq$95	8	805

TABLE 2. Collision outcomes selected from the experiments of Schaufelberger (R = 275, r = 200 μm, We = 1.14], arranged by increasing relative charge, showing number of coalescences [C] and bounces [B] in 25 equal cross sections by offset number (m).

Expt.	2	3	5	6	7	8
ΔQ, pC	0.004	0.012	0.050	0.063	0.076	0.26
Offset	Collision outcomes					
1	5C	1C	5C	7C	7C	2C
2	3C	1C	1C	8C	3C	1C
3	5C		3C	1C	3C	3C
4	5C	4C	6C	3C	8C	
5	3C	6C	4C	1C		
6	8C		2C	3C	2C	3C
7	7C	1C	4C	1C	6C	3C
8	5C		4C	6C	5C	1C
9	6C	3C	6C	4C	6C	1C
10	4C	3C, 2B	4C	6C	5C	3C
11	2C, 1B	1C, 2B	4C, 1B	4C	4C	1C
12	3B	1C, 1B	1C, 6B	1C	4C, 1B	3C
13	2B	1C, 1B	2C, 3B	1C, 2B	2C, 3B	2C
14	3B		1C, 2B	1C, 2B	1C, 1B	3C
15	4B	2B	3B	4C, 3B	2C, 1B	
16	4B	4B	3B	2B	5C, 1B	1C
17	6B	1C, 3B	1C, 2B	1C, 3B	2C, 2B	1C
18	2B	2B	1B	2C, 1B	3C	1C
19	4B	2C, 2B	1C, 3B	3C, 1B	2C	1C
20	2B	4B	2C, 3B	2C	2C	1C
21	5B	2B	1C, 4B	1B	6C, 1B	1C
22	1B	2B	4C, 1B	1B		4C
23	2B	1B		5C	4C	2C
24	3B	1C	3C	5C	1C	2C
25	1B		3C	2C	3C	4C

TABLE 3. Collision outcomes selected from the experiments of Laird (1992) (R = 425, r = 300 μm, We = 4.22], arranged by increasing relative charge, showing number of coalescences [C], bounces [B], and temporary coalescenes with number of satellites [T, T_1, T_2] in 25 equal cross sections by offset number (m).

Expt.	4	6	7	13	14	16
ΔQ, pC	0.029	0.19	0.40	1.2	2.5	4.7
Offset	Collison outcomes					
1	4C	5C	10C	7C	9C	6C
2	3C	11C	4C	10C	11C	4C
3	3C, 1B	3C	6C	10C	7C	4C
4	2C, 1B	7C, 3B	8C	10C	7C	7C
5	1C, 8B	3C, 7B	5C	16C	6C	3C
6	1B	4C, 7B	2C, 1B, 2T	10C	8C	3C
7	2B	1C, 6B	2C, 5T	7C	9C	8C
8	4B	4C, 3B	1C, 1B	4C	6C	2C
9	4B		2C, 1B, 1T, $1T_1$	8C	3C, 2T	5C
10	2B	1C, 2B	1C, 1B, 3T, $1T_1$	5C, 3T	2C, 3T	9C
11	4B	2B	6T, $4T_1$	3C, 4T, $2T_1$	1C, 1T, $1T_1$	1C
12	6B	4B, 1T	4T, $1T_1$, $1T_2$	1C, 1T, $1T_1$	2T, $2T_1$	4C
13	4B	4B, $1T_1$	1B, 2T	1C, $2T_1$	1T	4C
14	7B	12B	1B, 3T	$2T_1$	2T, $1T_1$	4C
15	3B	8B	3B, 6T, $1T_1$	7T, $1T_1$	2T	5C
16	6B	6B	1B, 3T, $3T_1$	3T	1T	4C
17	4B	5B	2B, $2T_1$	4T, $1T_1$	3T	3C
18	6B	4B	2B, 1T, $1T_1$	5T, $1T_1$	1C, 1T	4C
19	7B	2B	$2T_1$	1T		2C
20	2B	5B	$1T_1$	4T	2C	1C
21	9B	2B		2T	3C	1C
22			3T, $2T_1$		4C	2C
23	3B		3T	1C, 1T	1C	1C
24	1B		3T	1C, 1T	1C	2C
25	2B			1C		2C

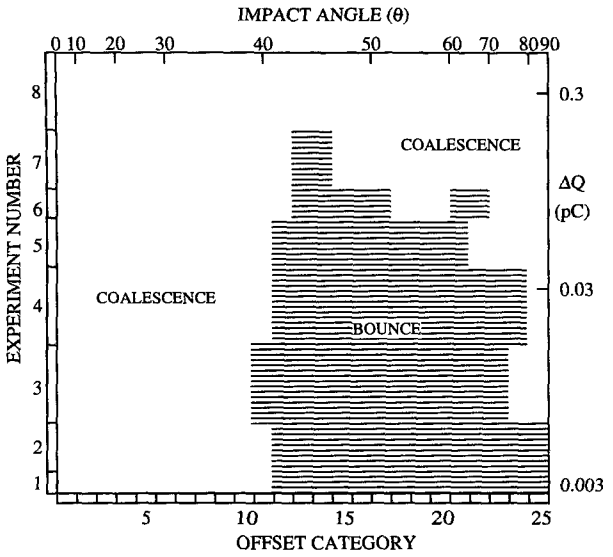

FIG. 5. Simplified collision outcomes from experiments of Schaufelberger (R = 275, r = 200 μm, We = 1.14), arranged by experiment number with increasing relative charge, showing majority regions of coalescence and bounce in 25 equal cross sections by impact-angle range.

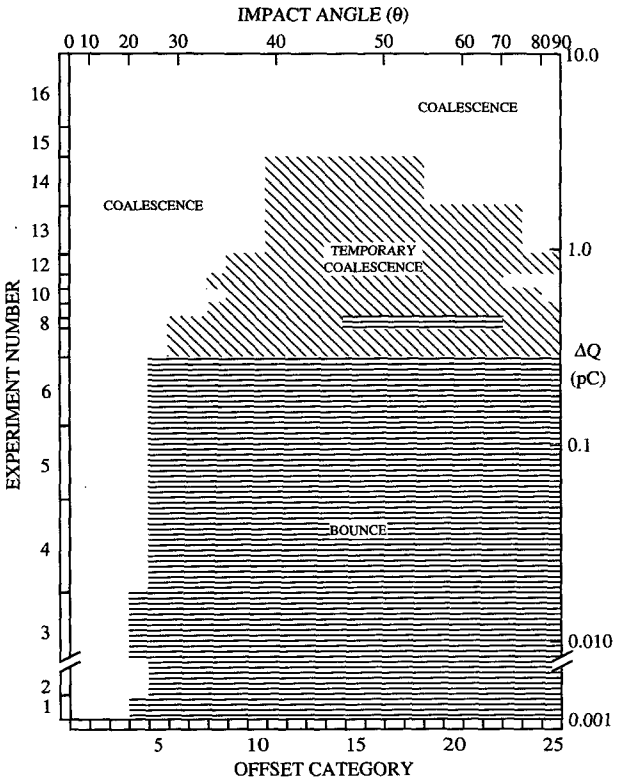

FIG. 6. Simplified collision outcomes for experiments of Laird (R = 425, r = 300 μm, We = 4.22), arranged by experiment number with increasing relative charge, showing majority regions of coalescence, bounce, and temporary coalescence in 25 equal cross sections by impact-angle range.

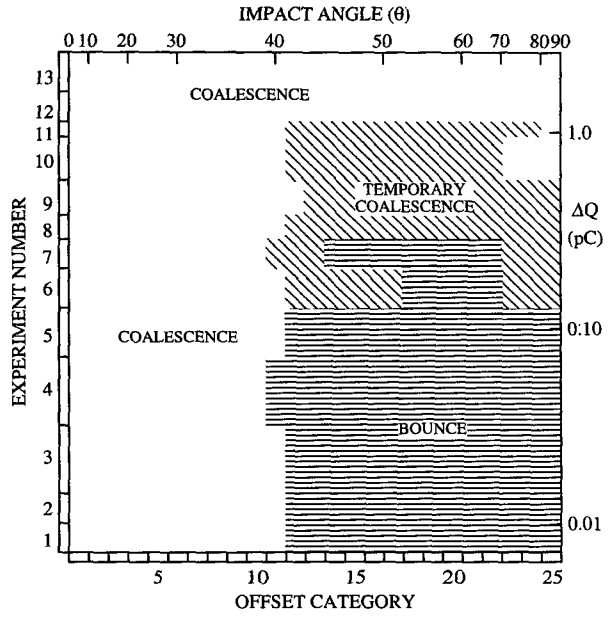

FIG. 7. Simplified collision outcomes for experiments of Czys (R = 340, r = 190 μm, We = 4.25), arranged by experiment number with increasing relative charge, showing majority regions of coalescence, bounce, and temporary coalescence in 25 equal cross sections by impact-angle range.

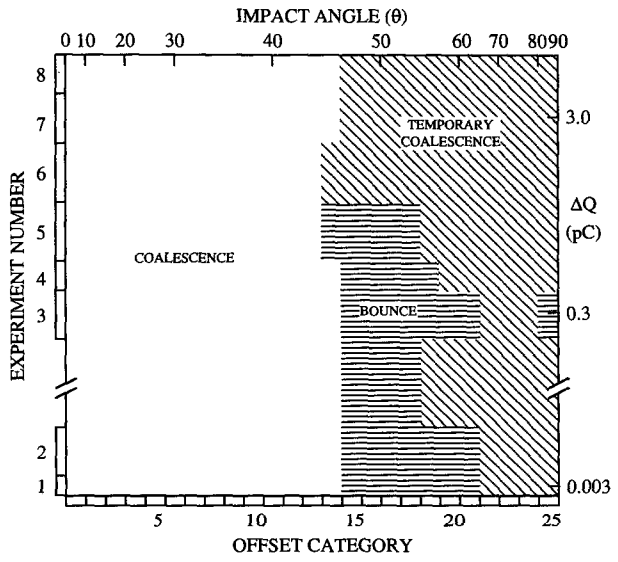

FIG. 8. Simplified collision outcomes for experiments of Holdridge (R = 425, r = 200 μm, We = 9.60), arranged by experiment number with increasing relative charge, showing majority regions of coalescence, bounce, and temporary coalescence in 25 equal cross sections by impact-angle range.

In our three studies at higher Weber number, many of the charge-induced coalescences were only temporary, because of the tendency for rotational separation at larger offset and higher Weber number (Brazier-Smith et al. 1972). This trend is confirmed by the highest Weber number study showing temporary coalescence even at the highest charge levels (Fig. 8).

In the low Weber number study of Schaufelberger, separation occurred only by bounce as it did in the previous low Weber number study of Ochs et al. (1986). Temporary coalescence in the higher Weber number studies occurred with up to two satellite drops from the collapsed filament connecting the separating drops. Satellites occurred across most of the regions of temporary coalescence in Figs. 6–8.

b. Satellite droplets

The distribution of satellite sizes are given in Table 4 by 10-μm categories of satellite radius. For collisions producing a single satellite, the number of size measurements and the size ranges were 59, 44–113 μm (Laird); 30, 48–113 μm (Czys): 63, 32–100 μm (Holdridge). Although not all satellite sizes could be measured, because of droplet distortion and movement out of the camera depth of field, the number of measurements was large enough to obtain a reasonable estimate for the single-satellite mean and interval of one standard deviation: 81 $\pm$ 15 μm (Laird); 65 $\pm$ 15 μm (Czys): 58 $\pm$ 12 μm (Holdridge).

For Holdridge's double-satellite events (14 out of 149 total satellite events), 13 satellites were measured. The range and means with the standard deviation interval were 55–105, 88 $\pm$ 15 μm for the larger satellite, and 50–66, 54 $\pm$ 5 μm for the smaller satellite. For the purpose of comparing data, the weighted average of Holdridge's single and double satellite size was used for the mean and standard deviation: 67 $\pm$ 13 μm. Double satellite events were also observed by Laird (7 out of 126 satellite events), but none were measurable. Overall, the dispersion of satellites sizes (one standard deviation range) for the self-collection studies was typically $\pm$15%–20% of the mean size.

The average satellite sizes for the present study are in the range of r_s = 58–81 μm. If the satellite formula of Brazier-Smith et al. (1973) is applied to our drop sizes, it predicts sizes of r_s = 62–93 μm, fairly close to our experimental results. Our satellite sizes are summarized in Table 5 for the mean of all measured satellite droplets, the standard deviation (σ_s), and the size predicted by the formula of Brazier-Smith et al. (1973) from measurements using colliding drop streams: $r_s' \approx 0.34r(1 + p^3)^{1/3}$. Further analysis of the size and number of satellites will be presented in Part 2 along with estimates of mass transfer for collisions involving temporary coalescence.

c. Collisions at large offset

Occasionally an offset was measured that was larger than $R + r$. This was rare, occurring an average of once every two experiments—that is, only 27 times out 4200 collisions during the 45 experiments. Most of these 27 events are a result of the rms measurement error of 2 μm. An additional source of error is converging fall streaks. If the angle between the fall streaks is assumed to be the maximum in the experiment of 0.5°, then a measurement of the offset at a distance of $R + r$ above the collision (Fig. 1) would give an extra offset of $\delta x = (R + r)\sin(0.5°) = 0.02\,(R + r)$. This increase in offset by the converging streaks is about one offset category, because the boundaries for offset 25 are 0.98 $(R + r)$ and 1.00 $(R + r)$. It is therefore likely that some of the offsets larger than $R + r$ may have occurred because of converging streaks. This error (δx) due to converging fall streaks would occur at other offsets as well. However, such a small offset error in the collision outcomes will not significantly affect the interpretation of the results.

Another peculiarity at large offset is a diminished number of recorded events. For example, in the study of Laird for experiment 6 (Table 3), there were no outcomes recorded above offset 22 (impact angles $\geq$ 66°). The lower number of outcomes at large offset is evident in all studies, for example, see also Table 2 as well as complete outcome tables in the appendix. The simplest explanation for this effect is alignment of the drops such that the more direct collisions are favored. Alignment was done to increase the collision rate, otherwise an experimental run could not

TABLE 4. Satellite size distribution by number measured in 10-μm categories of satellite radius for single satellite events and double satellite events (with separate distributions for the large and small satellite sizes).

	Boundaries (μm)									
	30	40	50	60	70	80	90	100	110	120
Laird			2	3	8	12	17	12	4	1
Czys			2	14	6	5		2		1
Holdridge (single)		4	11	24	15	7	1		1	
Holdridge (double, large)					1			2	3	1
Holdridge (double, large)					5	1				

have been completed before the drift in drop generation would adversely affect the charge and the stability of the pulsed-out pairs.

Two factors support the "over-alignment" hypothesis. First, alignment was easier in the low-charge experiments as was evident by a greater frequency of recorded collisions. At higher charges, a larger horizontal motion was imparted to the drop by the deflection field so that "pulsed-out" drops were more difficult to align. The trend with charge is clearly revealed in the complete outcome tables (appendix) showing relatively more outcomes at large offset for higher charge. The second factor is that more outcomes at large offset were obtained in experiment 4 of Laird when the drops with low charge were purposely "misaligned" in comparison to experiment 6 (see Table 3). There was still a deficiency in outcomes at large offset in experiment 4, because some alignment was needed to obtain a practical collision rate.

Although alignment of the drop pairs reduced the number of outcomes at large offset, it did not affect the type of outcome. In general, the lack of data in any offset category, whether from overalignment or just by chance, did not present any major difficulties in interpreting the results. Most of the data gaps could be filled by simple interpolation as discussed in the appendix.

d. *Coalescence efficiencies*

As is evident from Figs. 5–8, each experiment has a nearly constant offset dividing the coalescence outcomes from bounce and temporary coalescence outcomes. The low-charge contributions to the coalescence efficiency by the central coalescence region, using critical impact angles (θ_c) from Figs. 5–7, are $\epsilon_c = \sin^2 40° = 0.41$ (Schaufelberger and Czys), $\sin^2 20° = 0.12$ (Laird), and $\sin^2 46° = 0.52$ (Holdridge). These values are slightly lower than the coalescence efficiency, because of a few permanent coalescences at impact angle beyond the central region of coalescence.

The coalescence efficiency was determined in each of the 45 experiments from the fractional number of permanent coalescences in each offset category: $\Delta\epsilon_m = 4\%[N_C/(N_C + N_B + N_T)]_m$, where N_C, N_B, and N_T denote the number of coalescences, bounces, and temporary coalescence in a particular offset category. Because each offset category is $1/25$ the cross section, each category contributes a maximum of 4% to the coalescence efficiency. The sum over $m = 25$ categories gave the total coalescence efficiency

$$\epsilon(\%) = \sum \Delta\epsilon_m(\%) = 4\% \sum [N_C/(N_C + N_B + N_T)]_m. \quad (7)$$

Any categories without observations were given the average fraction of coalescences based on adjacent categories. The outcomes found at offset just beyond category 25, due to measurement error, were placed into category 25.

The resulting coalescence efficiencies are shown in Fig. 9 for each study as a function the relative charge magnitude ΔQ. [Values of ϵ and ΔQ are given in Tables A1–A4 in the appendix.] The minimal-charge coalescence efficiencies are indicated by ϵ values and dashed lines. As is evident from Fig. 9, the coalescence efficiency increases with drop charge, but more charge is required to produce the same increase at higher Weber number. At highest Weber number (Holdridge), with the highest rotational energy (relative to the surface energy), the charge-induced coalescences in the bounce domain were only temporary (Fig. 8).

The plots on Fig. 9 illustrate that charge-induced coalescence can produce a significant increase in coalescence efficiency. For the low Weber number case of Schaufelberger, charge effects are evident at $\Delta Q \approx 0.01$ pC, but in the highest Weber number case of Holdridge charge effects are just noticeable at $\Delta Q \approx 1$ pC. In the intermediate Weber number cases of Laird and Czys, charge effects become evident for $\Delta Q = 0.2$–0.4 pC. The effect of drop polarity (same vs opposite) appears to be minimal.

Charges of magnitude greater than 0.01 pC are found only in well-electrified clouds, such as deep convection (see Fig. 9.6, Beard and Ochs 1986). Because the coalescence process is active in warm base deep convection, the results from our laboratories indicate that precipitation may be enhanced in developing thunderstorms by charge-induced coalescence or by increased satellite production (Ochs and Czys 1987).

The minimal-charge coalescence efficiencies are given in Table 6, obtained from the mean of N_ϵ values of ϵ at the lowest charge. The 95% confidence intervals for ϵ were in the range ± 1 to $\pm 3\%$. From Table 6 we see that the minimal-charge coalescence efficiencies in the self-collection regime do not vary in a simple way with either the Weber number or the size ratio. The table is organized by increasing We and decreasing p, but values of ϵ do not increase or decrease monotonically. The information we have to date suggests that at a constant size ratio ($p \approx 0.7$) the coalescence efficiency decreases with increasing Weber number, whereas at a constant Weber number (We ≈ 4.2) the coalescence efficiency decreases with increasing size

TABLE 5. Satellite results by increasing small drop size, giving the mean satellite size (r_S), standard deviation (σ_S), and the predicted satellite size r'_S from Brazier-Smith et al. (1973).

	R (μm)	r (μm)	r_S (μm)	σ_S (μm)	r'_S (μm)
Czys	340	190	65	13	62
Holdridge	425	200	68	13	66
Laird	425	300	81	15	93

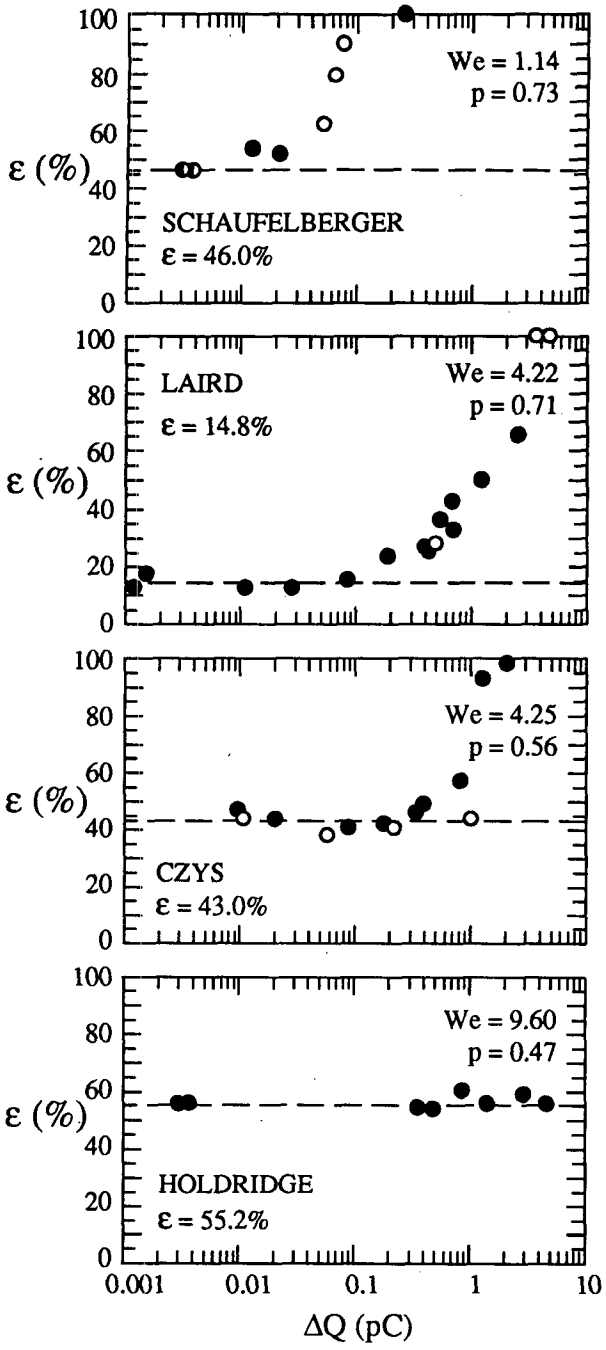

FIG. 9. Coalescence efficiencies as a function of relative-charge magnitude for the self-collection studies of Schaufelberger, Laird (1992), Czys, and Holdridge, arranged by increasing Weber number. Average minimal-charge coalescence efficiencies are stated on each diagram and shown by a dashed line. Drop pairs having charges of the same, opposite, and variable sign are identified by filled, hollow, and half-filled circles, respectively.

ratio. The relationship among ϵ, We, p will be developed in Part 2 using the intrinsic scaling from the collision dynamics.

5. Summary and conclusions

A general feature revealed by all studies was a coalescence region for small offset and a bounce region at intermediate-to-large offset and low-to-intermediate charge. The critical offset that separated the regions of coalescence and bounce was practically independent of charge. At higher charge values, increasing charge was found to induce permanent and/or temporary coalescence from smaller and larger offsets until bounce was completely eliminated. This effect was previously noted by Howarth and Crosby (1970). The collision outcomes of coalescence, bounce, and temporary coalescence are similar to earlier studies (Jayaratne and Mason 1964; Brazier-Smith et al. 1972). The more complex outcome patterns revealed in the present study have probably resulted from slight variations in offset and charge. Our results for freely falling drops should better reflect the natural variations in collision outcomes that occur in nature.

The application of our results to precipitation growth depends on the average outcome as a function of drop sizes and charges. Of particular interest is the coalescence efficiency. We obtained values for each of the 45 self-collection experiments from the fractional number of permanent coalescences in each offset category. The results were plotted as a function of charge to help determine the minimal-charge coalescence efficiencies of 15% to 55%. These efficiencies are significantly lower than previously reported for smaller drops in the self-collection regime (Ochs et al. 1986), and therefore indicate a further reduction in the growth rate of colliding precipitation drops. The production of satellite droplets found here, however, could have the effect of increasing the precipitation efficiency by providing embryos for additional raindrops (Langmuir 1948).

Our results indicate that charge-induced coalescence can produce a significant increase in coalescence efficiency. In the lowest Weber number study, charge effects were evident at $\Delta Q \approx 0.01$ pC, but in the higher Weber number studies charge effects were only noticeable above 0.1 pC. Charges of magnitude greater than 0.01 pC are found in well-electrified clouds, such as deep convection. Because the coalescence process is known to be active in warm base deep convection, precipitation may be enhanced in developing thunder-

TABLE 6. Average minimal-charge coalescence efficiency (ϵ) with 95% confidence interval (CI) by increasing Weber number and decreasing size ratio. Here N_ϵ is the number of lowest charge efficiencies in the average for ϵ.

	We	p	N_ϵ	ϵ (%)	CI (%)
Schaufelberger	1.14	0.73	2	46.0	—
Laird	4.22	0.71	5	14.8	2.1
Czys	4.25	0.56	5	43.0	2.8
Holdridge	9.60	0.47	4	55.2	1.4

TABLE A1. Collision outcomes and coalescence efficiencies for experiments of Schaufelberger (1990) (R = 275, r = 200 μm, We = 1.14], arranged by increasing relative charge, showing number of coalescences [C] and bounces [B] in 25 equal cross sections by offset category (m) and impact-angle range ($\Delta\theta$). First four rows are experiment number, relative charge, sign of charge, and character of relative humidity.

	Expt. num.	1	2	3	4	5	6	7	8
	ΔQ (pC)	0.003	0.004	0.012	0.021	0.050	0.063	0.076	0.26
	Sign Q q	±±	±±	−−	−−	+−	+−	+−	−−
	Rel. hum.	high	low	high	high	high	high	high	high
m	$\Delta\theta$ (deg)	Collision outcomes							
1	0.0–11.5	4*C*	5*C*	1*C*	4*C*	5*C*	7*C*	7*C*	2*C*
2	11.5–16.4	4*C*	3*C*	1*C*	7*C*	1*C*	8*C*	3*C*	1*C*
3	16.4–20.3	5*C*	5*C*		6*C*	3*C*	1*C*	3*C*	3*C*
4	20.3–23.6	8*C*	5*C*	4*C*	2*C*	6*C*	3*C*	8*C*	
5	23.6–26.6	6*C*	3*C*	6*C*	6*C*	4*C*	1*C*		
6	26.6–29.3	4*C*	8*C*		2*C*	2*C*	3*C*	2*C*	3*C*
7	29.3–31.9	8*C*	7*C*	1*C*	5*C*	4*C*	1*C*	6*C*	3*C*
8	31.9–34.4	8*C*	5*C*		4*C*	4*C*	6*C*	5*C*	1*C*
9	34.4–36.9	5*C*	6*C*	3*C*	6*C*	6*C*	4*C*	6*C*	1*C*
10	36.9–39.2	6*C*, 3*B*	4*C*	3*C*, 2*B*	6*C*	4*C*	6*C*	5*C*	3*C*
11	39.2–41.6	2*C*, 1*B*	2*C*, 1*B*	1*C*, 2*B*	3*C*, 1*B*	4*C*, 1*B*	4*C*	4*C*	1*C*
12	41.6–43.9	5*B*	3*B*	1*C*, 1*B*	3*C*, 5*B*	1*C*, 6*B*	1*C*	4*C*, 1*B*	3*C*
13	43.9–46.1	1*C*, 6*B*	2*B*	1*C*, 1*B*	3*B*	2*C*, 3*B*	1*C*, 2*B*	2*C*, 3*B*	2*C*
14	46.1–48.4	10*B*	3*B*		5*B*	1*C*, 2*B*	1*C*, 2*B*	1*C*, 1*B*	3*C*
15	48.4–50.8	3*B*	4*B*	2*B*	1*B*	3*B*	4*C*, 3*B*	2*C*, 1*B*	
16	50.8–53.1	11*B*	4*B*	4*B*	5*B*	3*B*	2*B*	5*C*, 1*B*	1*C*
17	53.1–55.6	6*B*	6*B*	1*C*, 3*B*	6*B*	1*C*, 2*B*	1*C*, 3*B*	2*C*, 2*B*	1*C*
18	55.6–58.1	5*B*	2*B*	2*B*	5*B*	1*B*	2*C*, 1*B*	3*C*	1*C*
19	58.1–60.7		4*B*	2*C*, 2*B*	6*B*	1*C*, 3*B*	3*C*, 1*B*	2*C*	1*C*
20	60.7–63.4	4*B*	2*B*	4*B*	5*B*	2*C*, 3*B*	2*C*	2*C*	1*C*
21	63.4–66.4	1*C*, 7*B*	5*B*	2*B*	1*C*, 4*B*	1*C*, 4*B*	1*B*	6*C*, 1*B*	1*C*
22	66.4–69.7	2*B*	1*B*	2*B*	4*B*	4*C*, 1*B*	1*B*		4*C*
23	69.7–73.6		2*B*	1*B*	1*B*		5*C*	4*C*	2*C*
24	73.6–78.5	2*C*, 3*B*	3*B*	1*C*	2*C*, 3*B*	3*C*	5*C*	1*C*	2*C*
25	78.5–90.0		1*B*			3*C*	2*C*	3*C*	4*C*
26	—	1*C*, 1*B*	4*C*	1*C*	1*C*	1*C*	1*C*	4*C*	
	Totals	65*C*	57*C*	27*C*	58*C*	63*C*	72*C*	90*C*	44*C*
		67*B*	43*B*	28*B*	54*B*	32*B*	16*B*	10*B*	
	ϵ (%)	46.0	45.9	54.7	51.9	62.6	75.6	90.2	100

storms by charge-induced coalescence or by increased satellite production (Ochs and Czys 1987).

The minimal-charge coalescence efficiencies in the self-collection regime do not vary in a simple way with either Weber number or size ratio. Our limited information suggests that at a constant size ratio ($p \approx 0.7$) the coalescence efficiency decreases with increasing Weber number, whereas at a constant Weber number (We $\approx$ 4.2) the coalescence efficiency decreases with increasing size ratio. Although ϵ does not vary in a simple way, we have been able to obtain an excellent fit to our laboratory data on coalescence efficiencies using the scaling intrinsic to inelastic collision theory. This analysis is presented in the companion paper Beard and Ochs (1995), where we also evaluate the size and number of satellites and estimate mass transfer for collisions involving temporary coalescence.

Acknowledgments. This research is based on work supported by the National Science Foundation under grant NSF ATM 9020959.

APPENDIX

Outcome Tables

a. Description of outcome tables

The collision outcomes from all four experiments are provided in Tables A1–A4. The first three rows give the experiment number by increasing charge, the relative charge magnitude, and the sign of the drop charges. In row four the relative humidity is characterized as "high" (≥95%) or low (21%–32%), except in Table A3, where the relative humidity was consistently high. The collision outcomes are tabulated by the number of observed coalescences (C), bounces (B), and temporary coalescences (T) with subscripts to indicated the number of satellites.

The collision outcomes in each table are placed in 25 equal cross sections by offset category (m) and impact-angle range ($\Delta\theta$). Collisions in category 26 occur at offsets greater than $R + r$, due to measurement error. At the bottom of each experiment column are the totals

TABLE A2. Collision outcomes and coalescence efficiencies for experiments of Laird (R = 425, r = 300 μm, We = 4.22], arranged by increasing relative charge, showing number of coalescences [C], bounces [B], and temporary coalescences with number of satellites [T, T_1, T_2] in 25 equal cross sections by offset category (m) and impact-angle range ($\Delta\theta$). First four rows are experiment number, relative charge, sign of charge, and character of relative humidity.

	Expt. num.	1	2	3	4	5	6	7	8	9	10	11	12	13	14	15	16
	ΔQ (pC)	0.0012	0.0015	0.011	0.029	0.086	0.19	0.40	0.42	0.50	0.54	0.68	0.72	1.2	2.5	3.6	4.7
	Sign Q q	−−	−−	−−	−−	−−	−−	−−	−−	+−	−−	−−	−−	−−	−−	−+	−+
	Rel. hum.	high	low	high	high	high	high	high	low	high	high	low	high	high	high	low	high
m	$\Delta\theta$ (deg)	Collison outcomes															
1	0.0–11.5	3*C*	6*C*	13*C*	4*C*	8*C*	5*C*	10*C*	4*C*	10*C*	8*C*	12*C*	5*C*	7*C*	9*C*	5*C*	6*C*
2	11.5–16.4	7*C*	4*C*	8*C*	3*C*	7*C*	11*C*	4*C*	6*C*	12*C*	9*C*	7*C*	5*C*	10*C*	11*C*	7*C*	4*C*
3	16.4–20.3	5*C*	8*C*, 1*B*	12*C*	2*C*, 1*B*	10*C*	3*C*	6*C*	9*C*	4*C*	6*C*	10*C*	7*C*	10*C*	7*C*	7*C*	4*C*
4	20.3–23.6	2*C*, 6*B*	1*C*	6*C*, 12*B*	2*C*, 1*B*	3*C*, 2*B*	7*C*, 3*B*	8*C*	8*C*	2*C*	2*C*	5*C*	7*C*	10*C*	7*C*	3*C*	7*C*
5	23.6–26.6	3*B*	1*C*, 2*B*	1*C*, 7*B*	1*C*, 8*B*	3*C*, 6*B*, 1*T*	3*C*, 7*B*	5*C*	4*C*, 1*B*	3*C*	4*C*	3*C*	5*C*	16*C*	6*C*	6*C*	3*C*
6	26.6–29.3	3*B*	1*C*, 3*B*	6*B*	1*B*	1*C*, 5*B*	4*C*, 7*B*	2*C*, 1*B*, 2*T*	1*C*, 1*B*, 2*T*	5*C*	6*C*	2*C*	6*C*	10*C*	8*C*	4*C*	3*C*
7	29.3–31.9	6*B*	1*B*	9*B*	2*B*	4*B*	1*C*, 6*B*	2*C*, 5*T*	1*C*, 2*T*	4*C*, 2*T*, 1T_1	6*C*, 1*T*	2*C*	5*C*, 1*T*	7*C*	9*C*	9*C*	8*C*
8	31.9–34.4	4*B*	7*B*	12*B*	4*B*	8*B*, 1*T*	4*C*, 3*B*	1*C*, 1*B*	1*C*, 1*B*	2*C*, 5*T*	3*C*, 2*T*	4*C*, 5*T*	2*C*, 1*T*	4*C*	6*C*	1*C*	2*C*
9	34.4–36.9	4*B*	4*B*	4*B*	4*B*	3*B*		2*C*, 1*B*, 1*T*, 1T_1	3*C*, 2*B*, 1*T*	1*C*, 4*T*	1*C*, 1*T*, 1T_1	2*C*, 4*T*	1*C*, 2*T*, 1T_1	8*C*	3*C*, 2*T*	6*C*	5*C*
10	36.9–39.2	9*B*	6*B*	7*B*	2*B*	6*B*	1*C*, 2*B*	1*C*, 1*B*, 3*T*, 1T_1	2*B*, 3*T*	6*T*	3*C*, 4*T*, 2T_1	2*T*, 1T_1	3*T*	5*C*, 3*T*	2*C*, 3*T*	3*C*	9*C*
11	39.2–41.6	12*B*	4*B*	5*B*	4*B*	2*B*	2*B*	6*T*, 4T_1	3*T*	2*T*	1*T*, 4T_1	3*T*, 1T_1	3*T*, 6T_1	3*C*, 4*T*, 2T_1	1*C*, 1*T*, 1T_1	3*C*	1*C*
12	41.6–43.9	3*B*	5*B*	5*B*	6*B*	3*B*	4*B*, 1*T*	4*T*, 1T_1, 1T_2	2*B*, 2*T*	3*T*	2*T*, 1T_1	7*T*	3*T*, 2T_1	1*C*, 1*T*, 1T_1	2*T*, 2T_1	7*C*	4*C*
13	43.9–46.1	3*B*	2*B*	2*B*	4*B*	3*B*	4*B*, 1T_1	1*B*, 2*T*	1*B*, 1*T*, 1T_1, 1T_2	2T_1, 1T_2	1*T*, 4T_1, 1T_2	4*T*	3*T*, 2T_1	1*C*, 2T_1	1*T*	4*C*	4*C*
14	46.1–48.4	7*B*	3*B*	10*B*	7*B*	2*B*	12*B*	1*B*, 3*T*	4*B*, 2*T*, 1T_1, 1T_2	5*T*	1*T*, 3T_1	2*T*, 3T_1	2*T*, 3T_1	2T_1	2*T*, 1T_1	3*C*	4*C*
15	48.4–50.8	3*B*	5*B*	4*B*	3*B*	13*B*	8*B*	3*B*, 6*T*, 1T_1	4*B*, 1T_1	1*B*, 2*T*, 1T_1	4*T*, 2T_1	2*T*, 5T_1	5*T*	7*T*, 1T_1	2*T*	6*C*	5*C*
16	50.8–53.1	6*B*	1*B*	1*B*	6*B*	4*B*	6*B*	1*B*, 3*T*, 3T_1	1T_1	2*T*, 1T_1	1*T*, 2T_1, 1T_2	4*T*, 1T_1	2*T*	3*T*	1*T*	2*C*	4*C*
17	53.1–55.6	6*B*	4*B*	3*B*	4*B*	3*B*	5*B*	2*B*, 2T_1	3*B*, 1T_1	1*B*, 2*T*, 1T_1	1*T*, 2T_1	2*T*	5*T*, 1T_1	4*T*, 1T_1	3*T*	1*C*	3*C*
18	55.6–58.1	2*B*	4*B*	2*B*	6*B*	4*B*	4*B*	2*B*, 1*T*, 1T_1	7*B*	1*T*, 1T_1	1*T*, 2T_1	4*T*, 1T_1	1*T*, 5T_1	5*T*, 1T_1	1*C*, 1*T*	3*C*	4*C*
19	58.1–60.7	3*B*	6*B*	3*B*	7*B*	2*B*	2*B*	2T_1	6*B*, 1T_1	2T_1, 1T_2	1T_1	3*T*	2T_1	1*T*			2*C*
20	60.7–63.4	3*B*	3*B*	1*B*	2*B*	1*B*	5*B*	1T_1	3*B*, 2T_1	1*B*, 1T_1	3*T*	3*T*	6*T*	4*T*	2*C*	2*C*	1*C*
21	63.4–66.4	2*B*	1*B*	1*B*	9*B*	1*B*	2*B*		4*B*	1*T*, 4T_1	1*T*	5*T*	5*T*	2*T*	3*C*	2*C*	1*C*
22	66.4–69.7	1*B*				1*B*		3*T*, 2T_1	1*B*	2T_1		2*T*	4*T*		4*C*	4*C*	2*C*
23	69.7–73.6				3*B*			3*T*	2*T*	1T_1		1*C*		1*C*, 1*T*	1*C*		1*C*
24	73.6–78.5				1*B*			3*T*	3*T*	2*T*	2*T*		1*C*, 6*T*	1*C*, 1*T*	1*C*		2*C*
25	78.5–90.0				2*B*				3*T*	2*T*	1*C*		2*C* 3*T*	1*C*		2*C*	2*C*
26	—							1*T*									
	Totals	17*C* 86*B*	21*C* 62*B*	40*C* 94*B*	12*C* 87*B*	32*C* 73*B* 2*T*	39*C* 82*B* 1*T*, 1T_1	41*C* 14*B* 46*T*, 19T_1, 1T_2	37*C* 42*B* 24*T*, 8T_1, 2T_2	43*C* 3*B* 39*T*, 17T_1, 2T_2	49*C* 26*T*, 24T_1, 2T_2	48*C* 52*T*, 12T_1	46*C* 55*T*, 22T_1	95*C* 37*T*, 10T_1	81*C* 18*T*, 4T_1	90*C*	91*C*
	ϵ (%)	13.0	17.9	13.8	13.8	15.5	23.2	27.0	25.5	28.4	36.5	43.1	33.2	50.5	65.3	100	100

TABLE A3. Collison outcomes and coalescence efficiencies for experiments of Czys (R = 340, r = 190 μm, We = 4.25), arranged by increasing relative charge, showing number of coalescences (C), bounces (B), and temporary coalescences with number of satellites (T, T_1) in 25 equal cross sections by offset category (m) and impact-angle range ($\Delta\theta$). First three rows are experiment number, relative charge (ΔQ), and sign of charges. Relative humidities were high (≥95%) in all experiments.

	Expt. num.	1	2	3	4	5	6	7	8	9	10	11	12	13
	ΔQ, pC	0.009	0.011	0.020	0.057	0.087	0.17	0.22	0.33	0.39	0.82	1.0	1.3	2.1
	Sign (Qq)	++	+−	++	−+	++	++	−+	++	++	++	−+	++	++
m	$\Delta\theta$ (deg)	Collision outcomes												
1	0.0–11.5	3C	5C	3C	5C	8C	9C	6C	7C	5C	8C	4C	1C	15C
2	11.5–16.4	3C	1C	2C	1C	4C	8C	1C	1C	3C	8C		3C	6C
3	16.4–20.3	3C	3C	2C		7C	8C	2C	2C	4C	3C	1C	1C	7C
4	20.3–23.6	1C	1C	1C	4C	5C	2C	2C	1C	5C	2C	2C	1C	8C
5	23.6–26.6	1C	3C	3C		4C	9C	3C	1C	3C	5C	2C	1C	11C
6	26.6–29.3	2C	2C	5C	4C	2C	5C	2C	4C	4C	5C	1C	6C	6C
7	29.3–31.9	4C	4C		1C	1C	12C	1C	2C	5C	3C	3C	3C	8C
8	31.9–34.4	3C	2C	3C		5C	7C	5C	1C	4C	3C	1C	1C	5C
9	34.4–36.9	3C	4C	1C	3C	2C	6C	3C	2C	5C	5C	2C	1C, 1T	5C
10	36.9–39.2	2C	3C, 1B		2C, 1B, 1T	2C	6C	3C	2C	3C	2C			2C
11	39.2–41.6	1C	1C	1C	1B, 1T_1	3C, 2B	2C, 1T_1	1T_1	1C	2C	2C, 1T	1C	2C	5C
12	41.6–43.9	2C, 3B	1C, 3B	5B	2B	1B	3T_1		1C, 1T_1	2C	4T		1C, 1T_1	5C, 1T_1
13	43.9–46.1	1C, 1B	5B	2B, 1T	1B, 1T_1	5B	1T, 4T_1	1T_1	1T	5T	1C, 3T	3T	4C	12C
14	46.1–48.4		4B	3B	3B	6B	7T_1	1B	1T_1		2T	1T	1C	6C
15	48.4–50.8	3B	2B	2B		3B, 1T_1	2T_1		1T	1T	4T	1T_1	4C, 1T	6C
16	50.8–53.1	4B	3B			1B, 1T_1	3T_1	2B		4T	4T	1T_1	2C, 1T	9C
17	53.1–55.6	1B	2B	2B	1B	3B	3T_1	2B	1T_1	2T, 3T_1	4T	1T_1	1C	6C
18	55.6–58.1		3B		3B	3B	3B, 3T_1	1B, 1T_1	1T_1	2T	3T	1T, 3T_1	5C	9C
19	58.1–60.7	3B	1B	1B	3B	2B	2B, 2T_1	1B	1T	2T	2C, 3T	2T_1	3C	5C
20	60.7–63.4		5B		1B	2B	4B	1C, 3B	3B, 1T_1	1C, 2T	1T	2T_1	1C	2C
21	63.4–66.4	1B	2B		6B	4B	2B, 1T	1B		2T, 2T_1	3C, 4T	1T, 1T_1	1C	4C
22	66.4–69.7		1B		2B		1B, 2T	1B	2T_1	1T, 1T_1	1T	1T, 2T_1	3C	2C
23	69.7–73.6		3B				3B, 2T				2C, 1T	2T		6C
24	73.6–78.5						5T	1T		2T,1T_1	3C	1T, 2T_1		3C
25	78.5–90.0		1B				2T		4T_1	1T	1C			3C
26	—													1C, 2T
	Totals	29C 16B	30C 36B	21C 15B 1T	20C 24B 1T, 2T_1	43C 32B 2T_1	74C 15B 13T, 28T_1	29C 12B 1T, 3T_1	25C 3B 3T, 11T_1	46C 24T, 7T_1	58C 35T	17C 10T, 15T_1	46C 3T, 1T_1	157C 2T, 1T_1
	ϵ (%)	47.6	44.0	44.0	38.0	41.6	42.7	41.0	46.0	49.3	57.7	44.0	92.9	98.0

for each type of outcome and the coalescence efficiency computed from the fractional number of coalescences in each offset category according to Eq. (8).

These tables show complicated outcome patterns, in part, because of insufficient outcomes in some offset categories. Many categories contain only one or two observations of a particular type; therefore, it is impossible to fix with any certainty the percentage occurrence for each type in such categories. This problem is similar to determining the overall percentage of heads and tails with just a few tosses of a coin. By chance, some offset categories were empty, particularly where the average number of outcomes was low at larger offsets. Empty categories can justifiably be filled by interpolation in regions containing one type of outcome, for example, gaps in coalescence (Table A1, experiment 3) for categories 3, 6, 8, and 25. Extrapolation would also be appropriated in single outcome regions, such as bounces for categories ≥ 22 in Table A3, experiments 1–5.

To obtain simplified diagrams for discussing the results in section 4, the majority (or plurality) outcome was determined for each offset category, followed by simple interpolation and extrapolation as just described. Although the resulting diagrams (Figs. 5–8) are much simpler than the Tables A1–A2, some ragged boundaries remain because the majority is uncertain at the border with nearly equal numbers of two outcomes. For example, the transition from coalescence to bounce in experiment 1 of Schaufelberger (Table A1) occurred near offset 11. The outcomes for offsets from 9 to 14 were (5C), (6C, 3B), (2C, 1B), (5B), (1C, 6B), (10B), and a simple majority determination put the boundary between the categories 11 and 12. In experiment 2 the outcomes for offsets 10–12 were (4C), (2C, 1B), and (3B), so the border was also between categories 11 and 12. In experiment 3 the placement of the border was less certain because the outcomes for offsets 9–13 were (3C, 2B), (1C, 2B), (1C, 1B), (1C, 1B). The majority decision placed the border be-

TABLE A4. Collision outcomes and coalescence efficiencies for experiments of Holdridge (R = 425, r = 200 μm, We = 9.60], arranged by increasing relative charge, showing number of coalescences [C], bounces [B], and temporary coalescences with number of satellites [T, T_1, T_2] in 25 equal cross sections by offset category (m) and impact-angle range ($\Delta\theta$). First four rows are experiment number, relative charge, sign of charge, and character of relative humidity.

	Expt. num.	1	2	3	4	5	6	7	8
	ΔQ (pC)	0.003	0.004	0.35	0.49	0.87	1.4	3.0	4.6
	Sign Q q	±±	−±	−−	−−	−−	−−	−−	−−
	Rel. hum.	low	high	high	high	high	high	high	high
m	$\Delta\theta$ (deg)	Collision outcomes							
1	0.0–11.5	6*C*	6*C*	13*C*	6*C*	2*C*	7*C*	8*C*	3*C*
2	11.5–16.4	9*C*	6*C*	4*C*	4*C*	3*C*	3*C*	7*C*	3*C*
3	16.4–20.3	5*C*	5*C*	7*C*	8*C*	3*C*	1*C*	5*C*	4*C*
4	20.3–23.6	2*C*	5*C*	8*C*	2*C*	5*C*		3*C*	4*C*
5	23.6–26.6	6*C*	4*C*	6*C*	4*C*	6*C*	2*C*	7*C*	4*C*
6	26.6–29.3	5*C*	4*C*	8*C*	1*C*	6*C*	5*C*	2*C*	2*C*
7	29.3–31.9	4*C*	7*C*	3*C*	4*C*	2*C*		4*C*	4*C*
8	31.9–34.4		5*C*	5*C*	2*C*	5*C*	1*C*	3*C*	8*C*
9	34.4–36.9	4*C*		4*C*	4*C*	1*C*	3*C*	5*C*	2*C*
10	36.9–39.2	4*C*	2*C*	6*C*	4*C*	5*C*	7*C*	5*C*	5*C*
11	39.2–41.6	3*C*	2*C*	5*C*	2*C*	3*C*	4*C*	5*C*	5*C*
12	41.6–43.9	10*C*	5*C*	9*C*	3*C*	3*C*	4*C*	8*C*	5*C*
13	43.9–46.1	3*C*	5*C*	5*C*	2*C*	7*C*	1*C*	6*C*	6*C*
14	46.1–48.4	4*C*, 1*T*	3*C*, 1*B*	3*C*, 1*B*, 1*T*	3*C*, 1*B*	1*C*, 3*B*	$1T_1$	2*C*, 1*T*, $1T_1$	3*C*, $1T_1$
15	48.4–50.8	1*C*, 4*B*	1*C*, 2*B*	1*B*, 1*T*	1*C*, 3*B*	3*C*, 5*B*	$4T_1$	2*C*, 1*T*, $4T_1$	1*C*, $3T_1$
16	50.8–53.1	7*B*	2*B*	4*B*, 1*T*	6*B*	6*B*	1*C*	1*C*, 1*T*, $2T_1$	$3T_1$
17	53.1–55.6	4*B*	7*B*, 1*T*	1*T*	2*B*	2*B*, 1*T*	$1T_1$	1*C*, $1T_1$	3*T*, $2T_1$
18	55.6–58.1	1*B*	3*B*, 1*T*	2*B*, 1*T*, $1T_1$	4*B*, $2T_1$	1*B*, $1T_1$	$6T_1$	1*C*, 2*T*, $3T_1$	1*T*, $3T_1$
19	58.1–60.7	5*B*, 1*T*	2*T*, 2*T*, $1T_1$	3*B*	3*B*, $1T_1$	4*T*, $3T_1$, $1T_2$	$4T_1$	2*T*, $2T_1$	1*T*, $1T_1$
20	60.7–63.4	4*B*, 1*T*	1*B*, 1*T*, $1T_1$	2*B*	1*B*, 3*T*, $1T_1$	1*C*, 4*T*, $2T_1$	$2T_1$	3*T*, $1T_1$	2*T*, $1T_2$
21	63.4–66.4	1*B*, $1T_1$	1*B*	4*B*, 2*T*	2*B*, 1*T*, $2T_1$	1*C*, $2T_1$	$3T_1$	1*T*, $4T_1$	2*T*, $3T_1$, $1T_2$
22	66.4–69.7	1*B*, 1*T*, $1T_1$	1*B*, $4T_1$	$1T_1$	$1T_1$	1*C*, $5T_1$	1*T*, $3T_1$	2*T*, $4T_1$	$2T_1$
23	69.7–73.6		1*B*, $2T_1$		$2T_1$	1*C*, $1T_1$, $1T_2$	$5T_1$	1*T*, $4T_1$, $1T_2$	1*T*, $2T_1$, $2T_2$
24	73.6–78.5		1*T*, $1T_1$			1*C*, $1T_1$	$2T_1$	2*T*, $4T_1$, $2T_2$	$1T_1$, $1T_2$
25	78.5–90.0	$2T_1$	$2T_1$		$1T_1$	$3T_1$	$3T_1$, $2T_2$	$1T_1$, $1T_2$	$1T_2$
26	—			2*B*	$1T_1$		$1T_1$	1*T*	$3T_1$
	Totals	66*C* 27*B* 4*T*, $3T_1$	60*C* 21*B* 6*T*, $11T_1$	86*C* 19*B* 7*T*, $2T_1$	50*C* 22*B* 4*T*, $11T_1$	60*C* 17*B* 9*T*, $18T_1$, $2T_2$	39*C* 1*T*, $35T_1$, $2T_2$	75*C* 17*T*, $31T_1$, $4T_2$	59*C* 10*T*, $24T_1$, $6T_2$
	ϵ (%)	56.0	56.3	54.4	54.0	60.4	56.0	58.8	56.0

tween category 9 and 10. The border may lie closer to category 11, as it was for experiments 1 and 2, because the majority outcome of bounce in category 10, having (1*C*, 2*B*), could have occurred by chance, for example, in a series of three trials the sequences (1*C*, 2*B*) and (2*C*, 1*B*) each occur three out of eight times when the chance of observing *C* and *B* is equal. Thus, the shift in the border in Fig. 5 for experiment 3 is not significant, and such ±1 category variations in the borders between outcome regions seen in Figs. 5–8 are generally insignificant.

In the earlier study by Jayaratne and Mason (1964) using a supported large drop, they found two broad regions each for coalescence and bounce in the order *CBCB* from small to large offset. Our complete outcome tables for freely falling drops show considerably more structure in many of the experiments, for example, the results of most experiments in Schaufelberger's study appear to be *CBCBC* and *CBCBCBC*. Some of the structure results from gaps in outcome regions because of an insufficient number of observations. The most complicated results in Schaufelberger's study would reduce to a sequence of *CBCBC* by interpolation between nearby categories (Fig. A1). The majority outcome procedure used to construct Figs. 5–9 further simplifies the results by eliminating areas containing multiple outcomes—for example, the outcome sequences for Schaufelberger's are reduced to *CBC* and *CB* (Fig. 5).

b. *Explanation of multiple outcomes*

It is important to consider these regions of multiple outcomes further because such results appear to clash with our deterministic expectation of a single outcome at one offset for a particular pair of drop sizes and charges. The multiple outcomes in Tables A1–A4 occur in transition zones between larger regions of single

outcomes (C, B, T). In some cases all three outcomes were found in one category. The simplest explanation is an outcome transition within an offset category. Another is a transition near an offset boundary affecting two offset categories because of measurement error. Outcome transitions induced by charge would similarly produce multiple outcomes, but across experiments of different ΔQ.

There was a total of about 40 horizontal multiple-outcome regions with about half being two offsets wide. Thus, a single offset transition could explain about half of the multiple-outcome regions. Of the regions greater than two categories wide, about half did not extend across experiments so that a charge-induced transition *within the experiment boundary* would account for these regions. The remaining multiple-outcome regions overlapped adjacent experiments (having lower and higher charge) by only 1–2 offsets, so that the offset transitions could have spread across experiments. In a few of Laird's experiments, where the difference in charge between experiments was small, a charge-induced transition could have spread across several experiments (the average difference in ΔQ between adjacent runs from experiments 8–12 was only 4%).

The above explanation for multiple offsets requires large enough errors that a transition near an offset or charge boundary would spread into another category. The stated microscope accuracy for the offset is small (± 2 μm) when compared to the width of the offset categories: 10–95 μm (Schaufelberger, $R + r = 475$ μm), 16–155 μm (Laird, $R + r = 725$ μm). Because of impact angle variations, there is an additional offset error of about $0.02(R + r) = 10$–16 μm (see section 4c). The bounds in the offset errors are, therefore, about the ± 0.1 to ± 1.0 category from the smallest to largest offset. This is sufficient to cause spreading of an offset transition across one category, more so at larger offsets.

In Figs. 5–8 and Tables A1–A4 the charge width for most experiments is $\pm 0.3\Delta Q$ or less. Thus, extreme charge fluctuations must be somewhat larger than $\pm 0.3\Delta Q$ to spread outcome transitions across experiments (e.g., spread the outcomes vertically in Figs. 5–8). Usually, the mean charge was based on several measurements before and after each roll of film to insure that the charges were stable. Because only one representative measurement was recorded before and after, the 95% confidence interval in the mean for $n = 2$ is about three standard deviations, for example, the confidence interval is $\pm 0.3\Delta Q$ for $\sigma = 0.1\Delta Q$. The average ΔQ for an entire experiment, however, was based on about 25 rolls of film, so the confidence interval would be much narrower even with twice the standard deviation—for example, the confidence interval is $\pm 0.1\Delta Q$ for $n = 25$ and $\sigma = 0.2\Delta Q$. This latter confidence interval was typical for an entire experiment. Individual runs, however, had significantly larger confidence intervals. It is this larger range in ΔQ that would have contributed to the spreading of the outcomes vertically.

Furthermore, runs were discarded if the charge were found to fluctuate from beginning to end. Thus, the mean ΔQ for an entire experiment was compiled from selected runs having nearly the same ΔQ. While this procedure eliminated the collision results with obvious charge fluctuations, it also may have eliminated some of the larger variance intrinsic to the experiment. Thus, a bound of $\pm 0.3\Delta Q$, and occasionally somewhat greater, is not unreasonable for a particular roll of film, even with a confidence interval of $\pm 0.1\Delta Q$ in the mean for an entire experiment.

Because the uncertainty in the representative charge and offset can result in a spreading of outcome types from one region into another, the actual outcomes are probably simpler than in Tables A1–A4, but not as simple as in Figs. 5–8.

If multiple outcomes occur as result of experimental uncertainty in offset and charge, then our results are consistent with a "determinism" hypothesis that only one outcome occurs at one offset for a particular pair of drop sizes and charges. In effect, a placement error of an observed outcome resulted in the spreading of the outcome region beyond its borders in both the offset and charge direction. A modification of the determinism hypothesis is that some of the results may be subject to chaos—for example, charge-induced coalescence may be highly sensitive to offset and charge resulting in a fine (fractal) structure. Drop stream experiments with repeated collisions at practically the same offset and charge show only broad regions of collision outcomes, separated by relatively sharp borders (e.g., Park 1970). Thus, the hypothesis of determinism without chaos would seem more appropriate for the outcome of collisions between small precipitation drops.

c. *Discussion of outcome patterns*

In considering the majority outcomes for Schaufelberger at low charge in Fig. 5, we find coalescence at small offsets and bounce at large offsets (a "*CB*" sequence). The complete outcomes in Table A1, show an additional region of coalescence at the largest offset, and in some experiments another coalescence region within the bounce region. Thus, the low-charge sequence for the drop sizes of Schaufelberger seems to be either *CBC* or *CBCBC*.

The largest offset coalescences in these sequences are probably induced by charge. This is consistent with the trend in Fig. 5 of charge-induced coalescence (downward from higher charge) and the known influence of charge on coalescence (Howarth and Crosby 1970). Also, the low-charge data are close to the value needed to influence the coalescence efficiency (see Fig. 9). (The coalescence efficiency analysis in Part 2 also

shows that these coalescences are charge induced.) If we eliminate the supposed charge effect, the negligible-charge sequence in Schaufelberger's study would be the same as found by Jayaratne and Mason (1964): *CBCB*.

In summary, the low Weber number study of Schaufelberger is characterized by 1) a coalescence region for smaller offsets, 2) a bounce region having zero-to-one subregions of coalescences at intermediate-to-large offsets, 3) a coalescence region at large-offsets increasing inward with charge, and 4) a coalescence region for all offsets at high charge.

A notable feature of Table A1 is that charge-induced coalescence occurs at different locations within the bounce region for different experiments. Thus, the offset range for charge-induced coalescence appears to be a sensitive function of ΔQ. This is consistent with the three higher Weber number studies also having complicated patterns for charge-induced permanent and temporary coalescence.

In the intermediate Weber number study of Laird, the low-charge sequence was *CB* as seen in Table A2 and Fig. 6. There is no evidence of charge-induced coalescence for experiments 1–4, and no reason to expect it, because the low-charge data are well below the value observed to influence the coalescence efficiency (Fig. 9). Charge effects first appear as temporary coalescence in experiment 5 just inside the bounce region. The complex results for the intermediate charge experiments 7–10 are a consequence of low counts for bounce and temporary coalescence near the charge-induced (vertical) transition between them (see Fig. 6). Charge fluctuations of $\pm 0.3\Delta Q$ within individual runs would have been large enough to have spread bounces and temporary coalescences between experiments 7–10.

The lowest offset for temporary coalescence changes with increasing charge, occurring in offsets 5, 12, 6, 5, 7, and generally increasing thereafter to 9. This complicated ΔQ sensitivity of charge-induced coalescence occur in all the studies.

Another influence in the measurements of Laird is relative humidity. For example, the low relative humidity in experiment 8 caused significantly more bounces compared with the adjacent high relative humidity experiments 7 and 9 (see Table A2). The relative humidity effect has been attributed to a slower drainage of the air film between the drops at the reduced film temperature because of evaporative cooling (Ochs et al. 1995). In experiment 11 the effect of low relative humidity was to decrease the temporary coalescence events that produced satellite droplets (see Table A2).

In summary, the intermediate Weber number study in Table A2 is characterized by 1) a coalescence region for the smallest offsets, 2) a bounce region at intermediate-to-large offset and low charge, 3) a bounce region at intermediate-to-large offsets having one subregion of temporary coalescence at intermediate charge, 4) a temporary coalescence region at intermediate-to-large offset and intermediate charge, having two, one, and zero subregions of bounce with increasing charge, and 5) a coalescence region for all offsets at high charge.

The outcomes in Table A3 for the intermediate Weber number study of Czys at low charge have a "*CB*" sequence. As the charge increases, temporary coalescence appears at intermediate offsets in sequences of *CTB* and then at the largest offsets as *CTBT* (see also Fig. 7). For still higher charge, bounce is eliminated in sequences of *CT* and *CTC*, until practically all the outcomes are complete coalescences. As in the other studies, charge-induced coalescence is a sensitive function of ΔQ. The general features of Table A3 are similar to the other intermediate Weber number study of Laird, described above.

In the high Weber number study of Holdridge (Table A4, Fig. 8), temporary coalescence persisted at the highest charge, so the simplest sequence is *CT*. At lowest charge there are alternating zones for bounce and temporary coalescence. These complications result from the ΔQ sensitivity of charge-induced coalescence; the transition offset for temporary coalescence changes from category 13 to 17, twice, and then back to 13 with increasing charge. The effect of low relative humidity in experiment 1 for Holdridge was to increase the number of bounces and reduce the number of temporary coalescences compared with the adjacent high relative humidity experiment (see Table A4).

In summary, the high Weber number study in Table A4 is characterized by 1) a coalescence region for the smaller offset, 2) a bounce region at intermediate offset having one or two subregions of temporary coalescence at low-to-intermediate charge, 3) a temporary coalescence region at large offset and low-to-intermediate charge, and 4) a temporary coalescence region for intermediate-to-large offsets at high charge.

Another feature of our results, most apparent in the study of Czys, is that charged drops of the opposite and same polarity can produce different outcomes—for example, in Table A3 compare experiment 11 (*CT*) with experiments 10 and 12 (*CTC*). Other evidence that distinguishes between the polarity is a somewhat lower coalescence efficiency in the study of Czys for drop of the same polarity (Fig. 9). There is evidence in Table A3 that coalescences are more readily induced for drops having the same polarity of charge, because the transition between bounce and temporary coalescence occurs at a lower value of ΔQ, as does the transition between temporary coalescence and complete coalescence. The study of Schaufelberger was the only other one with a significant number of experiments having both polarities. The two sets of experiments appear to be generally similar, both displaying the general features seen in Fig. 5. In Part 2 of this study we will use the theory of Davis (1964) to develop a more complete

charge scaling that will help to reduce the scatter in coalescence efficiency as seen in Fig. 9.

A further complication in the outcome patterns may have resulted from differences in the relative magnitude of the charges. In the studies at higher ΔQ for Czys, Holdridge, and Laird, there was significantly more charge on the large drop than the small drop ($|Q| \gg |q|$), whereas in the study of Schaufelberger the magnitudes of the charges on the drop pair were comparable ($|Q| \approx |q|$) across the range of ΔQ values. Comparable charges were the normal situation at low ΔQ values in all studies. In a few experiments at intermediate ΔQ, the charge on the large drop was less than the small drop ($|Q| \ll |q|$): experiment 3 (Czys), experiments 4–6 (Schaufelberger) and experiment 4 (Laird). We could find no obvious effect of "peculiar" charges, such as $|Q| \ll |q|$ and $|Q| \approx |q|$. No experiments were done, however, *holding* ΔQ *constant* to test outcome difference for $|Q| \gg |q|$, $|Q| \ll |q|$, and $|Q| \approx |q|$.

REFERENCES

Adam, J. R., R. Cataneo, and R. G. Semonin, 1971: The production of equal and unequal size droplet pairs. *Rev. Sci. Instrum.*, **42,** 1847–1849.

Beard, K. V., 1977: On the acceleration of large water drops to terminal velocity. *J. Appl. Meteor.*, **16,** 1068–1071.

——, and H. T. Ochs, 1984: Collection and coalescence efficiencies for accretion. *J. Geophys. Res.*, **89,** 7165–7169.

——, and ——, 1986: "Charging mechanisms in clouds and thunderstorms." *The Earth's Electrical Environment, Studies in Geophysics,* National Research Council, National Academy Press, Washington, DC, 114–130.

——, and ——, 1995: Collisions between small precipitation drops. Part 2: Coalescence efficiency formulas for charged and uncharged drops. *J. Atmos. Sci.,* submitted.

Berry, E. X., and R. L. Reinhardt, 1974a: An analysis of cloud drop growth by collection. Part 1: Double distributions. *J. Atmos. Sci.*, **31,** 1814–1831.

——, and ——, 1974b: An analysis of cloud drop growth by collection. Part 2: Accretion and self-collection. *J. Atmos. Sci.*, **31,** 2118–2135.

Brazier-Smith, P. R., S. G. Jennings, and J. Latham, 1972: The interaction of falling water drops: Coalescence. *Proc. Roy. Soc. London A,* **325,** 393–408.

——, ——, and ——, 1973: Raindrop interactions and rainfall rates within clouds. *Quart. J. Roy. Meteor. Soc.*, **99,** 260–272.

Czys, R. R., 1987: A laboratory study of interaction between small precipitation-size drops in free fall. Ph.D. thesis, University of Illinois, Urbana-Champaign, IL, 131 pp.

——, and H. T. Ochs, 1988: The influence of charge on the coalescence of water drops in free fall. *J. Atmos. Sci.*, **45,** 3161–3168.

Davis, M. H., 1964: Two charged spherical conductors in a uniform electric field: Forces and field strength. *Quart. J. Mech. Appl. Math.*, **27,** 499–511.

de Almeida, F. C., 1977: Collision efficiency, collision angle and impact velocity of hydrodynamically interacting cloud drops: A numerical study. *J. Atmos. Sci.*, **34,** 1286–1292.

Gunn, R., 1965: Collision characteristics of freely falling water drops. *Science,* **150,** 695–701.

Holdridge, D. J., 1992: A laboratory investigation of electrostatic charge and relative humidity influences on the coalescence of precipitation size water drops. M. S. thesis, University of Illinois, Urbana-Champaign, IL, 89 pp.

Howarth, W. J., and E. J. Crosby, 1970: Effect of electrical charge on the coalescence of water drops in nitrogen. [Unpublished results given in Park (1970), 108–110.]

Jayaratne, O. W., and B. J. Mason, 1964: The coalescence and bouncing of water drops at an air/water interface. *Proc. Roy. Soc. London A,* **280,** 545–565.

Laird, N. F., 1992: A new investigation of relative humidity and electrostatic charge influences on the coalescence of precipitation drops. M. S. thesis, University of Illinois, Urbana-Champaign, IL, 98 pp.

Langmuir, I., 1948: The production of rain by chain reaction in cumulus clouds at temperatures above freezing. *J. Meteor.*, **5,** 175–192.

Ochs, H. T., and K. V. Beard, 1978: The collision efficiency of similarly sized precipitation drops. Preprints, *Conf. on Cloud Physics and Atmospheric Electricity,* Issaquah, WA, Amer. Meteor. Soc., 133–135.

——, and R. R. Czys, 1987: Charge effects on the coalescence of water drops in free fall. *Nature,* **327,** 606–608.

——, ——, and K. V. Beard, 1986: Laboratory measurements of coalescence efficiencies for small precipitation drops. *J. Atmos. Sci.,* **43,** 225–232.

——, D. E. Schaufelberger, and J. Feng, 1991: A reassessment of coalescence efficiency observations for small precipitation drops. *J. Atmos. Sci.,* **48,** 946–951.

——, K. V. Beard, N. F. Laird, D. J. Holdridge, and D. E. Schaufelberger, 1995: Effects of relative humidity on the coalescence of small precipitation drops in free fall. *J. Atmos. Sci.,* **52,** in press.

Park, R. W., 1970: Behavior of water drops colliding in humid nitrogen. Ph.D. thesis, University of Wisconsin, Madison, WI, 577 pp.

Prupacher, H. R., and J. D. Klett, 1978: *Microphysics of Clouds and Precipitation.* Reidel, 714 pp.

Sartor, J. D., and C. E. Abbott, 1972: Some details of coalescence and charge transfer between freely falling drops in different electrical environments. *J. Rech. Atmos.*, **6,** 479–493.

Schaufelberger, D. E., 1990: The influence of electrostatic charge and relative humidity on the coalescence of small free falling water drops. M. S. thesis, University of Illinois, Urbana-Champaign, IL, 78 pp.

Shafrir, U., and T. Gal-Chen, 1971: A numerical study of collision efficiencies and coalescence parameters for drop pairs with radii up to 300 microns. *J. Atmos. Sci.,* **28,** 741–751.